*Human Molecular Genetics*, 2021, Vol. 30, No. 23 2286–2299

https://doi.org/10.1093/hmg/ddab190
Advance Access Publication Date: 8 July 2021
General Article

GENERAL ARTICLE

# Molecular phenotyping and functional assessment of smooth muscle-like cells with pathogenic variants in aneurysm genes *ACTA2*, *MYH11*, *SMAD3* and *FBN1*

Joyce Burger[1,2,†], Natalija Bogunovic[3,4,5,†], Nathalie P. de Wagenaar[1,10], Hui Liu[6], Nicole van Vliet[1], Arne IJpma[2,6,7], Alessandra Maugeri[5], Dimitra Micha[5], Hence J.M. Verhagen[8], Timo L.M. ten Hagen[6], Danielle Majoor-Krakauer[2], Ingrid van der Pluijm[1,8], Jeroen Essers[1,8,9,‡,*] and Kak K. Yeung[3,4,‡,*]

[1]Department of Molecular Genetics, Oncode Institute, Erasmus University Medical Center, Rotterdam 3015 GD, The Netherlands, [2]Department of Clinical Genetics, Erasmus University Medical Center, Rotterdam 3015 GD, The Netherlands, [3]Department of Surgery, Institute for Cardiovascular Research, Amsterdam University Medical Centers, location VU University Medical Center, Amsterdam 1081 HV, The Netherlands, [4]Department of Physiology, Institute for Cardiovascular Research, Amsterdam University Medical Centers, location VU University Medical Center, Amsterdam 1081 HV, The Netherlands, [5]Department of Clinical Genetics, MOVE Institute, Amsterdam University Medical Centers, location VU University Medical Center, Amsterdam 1081 HV, The Netherlands, [6]Department of Pathology, Erasmus University Medical Center, Rotterdam , The Netherlands, [7]Department of Bioinformatics, Erasmus University Medical Center, Rotterdam 3015 GD, The Netherlands, [8]Department of Vascular Surgery, Erasmus University Medical Center, Rotterdam 3015 GD, The Netherlands, [9]Department of Radiation Oncology, Erasmus University Medical Center, Rotterdam 3015 GD, The Netherlands and [10]Department of Cardiology, Erasmus University Medical Center, Rotterdam 3015 GD, The Netherlands

*To whom correspondence should be addressed at: J. Essers, Erasmus Medical, Center, Room Ee702b, Wytemaweg 80, 3015 CN Rotterdam, PO Box 2040, 3000 CA Rotterdam 3015 GD, The Netherlands. Tel: +31 107043724; Fax: +31 107044743; Email: j.essers@erasmusmc.nl; K.K. Yeung, AUMC, location VUmc, De Boelelaan 1117, 1118, PO Box 7057, 1007 MB Amsterdam, The Netherlands. Tel: +31 614278725; Fax: +31 204441437; Email: k.yeung@amsterdamumc.nl

## Abstract

Aortic aneurysms (AAs) are pathological dilatations of the aorta. Pathogenic variants in genes encoding for proteins of the contractile machinery of vascular smooth muscle cells (VSMCs), genes encoding proteins of the transforming growth factor beta signaling pathway and extracellular matrix (ECM) homeostasis play a role in the weakening of the aortic wall. These variants affect the functioning of VSMC, the predominant cell type in the aorta. Many variants have unknown clinical significance, with unknown consequences on VSMC function and AA development. Our goal was to develop functional assays that show the effects of pathogenic variants in aneurysm-related genes. We used a previously developed fibroblast

[†]These authors contributed equally.
[‡]These authors contributed equally.

**Received:** May 5, 2021. **Revised:** June 25, 2021. **Accepted:** July 5, 2021

transdifferentiation protocol to induce VSMC-like cells, which are used for all assays. We compared transdifferentiated VSMC-like cells of patients with a pathogenic variant in genes encoding for components of VSMC contraction (*ACTA2*, *MYH11*), transforming growth factor beta (TGF$\beta$) signaling (*SMAD3*) and a dominant negative (DN) and two haploinsufficient variants in the ECM elastic laminae (*FBN1*) to those of healthy controls. The transdifferentiation efficiency, structural integrity of the cytoskeleton, TGF$\beta$ signaling profile, migration velocity and maximum contraction were measured. Transdifferentiation efficiency was strongly reduced in *SMAD3* and *FBN1* DN patients. *ACTA2* and *FBN1* DN cells showed a decrease in SMAD2 phosphorylation. Migration velocity was impaired for *ACTA2* and *MYH11* cells. *ACTA2* cells showed reduced contractility. In conclusion, these assays for showing effects of pathogenic variants may be promising tools to help reclassification of variants of unknown clinical significance in AA-related genes.

## Graphical Abstract

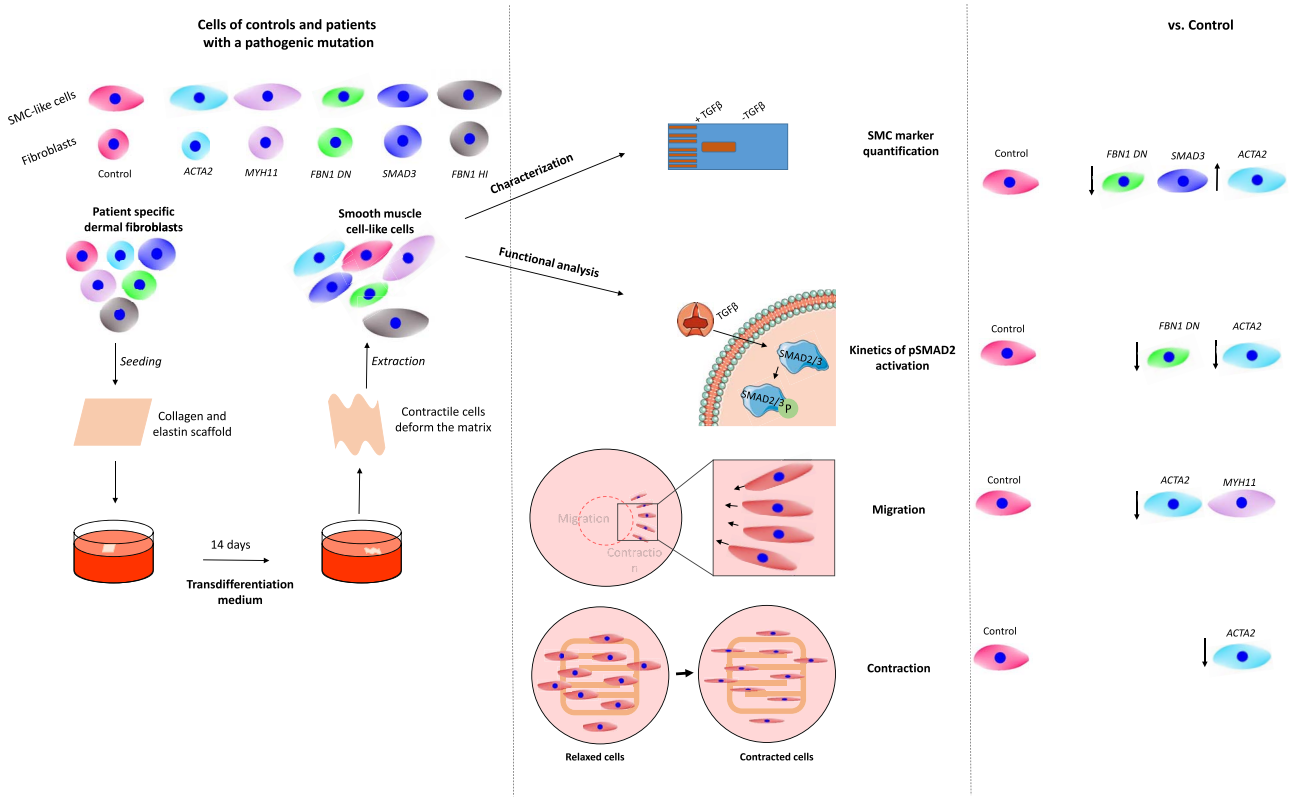


## Introduction

Aortic aneurysms (AA) are pathological dilatations of the aorta. AA can be life threatening in cases of untreated aneurysm growth leading to rupture, with a mortality rate of up to 80% (1). AA can occur in both segments of the aorta and are referred to accordingly as thoracic and abdominal AA. Genetic causes for thoracic and abdominal AA underlie syndromic and non-syndromic familial disease (2,3). AA may be caused by a variety of pathogenic variants in genes encoding structural components of the extracellular matrix (ECM), cytoskeletal/smooth muscle contraction proteins and proteins associated with the TGF$\beta$ signaling pathway. Pathogenic variants in the genes encoding the cytoskeleton/contractile machinery of vascular smooth muscle cells (VSMCs), such as *ACTA2* ($\alpha$-smooth muscle actin), *MYH11* (myosin heavy chain 11), *MYLK* (myosin light chain kinase) and *PRKG1* (Cyclic guanosine monophosphate (cGMP)-dependent protein kinase 1 alpha isozyme) (4–7) may lead to altered contractility of VSMCs. Aneurysm-related genes having an effect on the TGF$\beta$ signaling pathway are TGF$\beta$ receptor 1 (*TGFBR1*), *TGFBR2*, *TGFB2*, *TGFB3*, *SMAD2* and *SMAD3* (8–17). Pathogenic variants in aneurysm-related genes encode for components of the ECM and lead to disruption of the ECM homeostasis, resulting in a weakening of the aortic wall, loss of mechanical resilience, elasticity and altered ability to retain latent TGF$\beta$. Genes in this group include *FBN1* (encoding fibrilin-1), *COL3A1* (collagen type 3 $\alpha$1), *ELN* (elastin), *EFEMP2* (fibulin-4) and *LOX* (lysyl oxidase) (18–29).

The pathogenic mechanism underlying aneurysm formation is not fully understood. Mutations in the aforementioned genes affect the normal functioning of VSMC, such as their contractile properties, interaction with the ECM and TGF$\beta$ signaling. These mutations affect the ability of VSCMs to adapt to mechanical stimuli and subsequent expression of aneurysm-related genes (30). To study the effects of pathogenic variants in aneurysm-related genes affecting VSMC function *in vitro*, VSMCs can be isolated from aortic tissue retrieved from open aneurysm surgery. Alternatively, dermal fibroblasts grown on a scaffold containing collagen and elastin or coverslips can be transdifferentiated into VSMC-like cells within 2 weeks using TGF$\beta$1. This model has previously been tested and showed that VSMC-like cells were comparable with primary human aortic smooth muscle cell

(SMC) with regard to messenger RNA expression of SMC markers *ACTA2*, *SM22* and *CNN1* (31). The purpose of this study was to investigate and develop assays that can identify the molecular phenotype and measure effects of pathogenic variants, in order to have a panel of pathogenic signatures of aneurysm genes that can be used as reference for reclassification of variants of unknown clinical significance (VUS) in the aneurysm-related genes. To develop and validate these novel robust functional assays, we used VSMC-like cells of healthy controls and AA patients with a pathogenic variant in the AA-related genes [*ACTA2*, *MYH11*, *SMAD3*, *FBN1* haploinsufficient (HI) and dominant negative (DN)] and assessed their potential to differentiate, TGF$\beta$ signaling, migratory capacity and contractility.

## Results

### Assessment of baseline values for control VSMC-like cell transdifferentiation efficiency

Human dermal fibroblasts from three healthy donors were transdifferentiated into VSMC. A schematic overview of the transdifferentiation protocol is shown in Figure 1A. Transdifferentiation efficiency was determined by quantifying VSMC marker proteins. Western blot analysis of smooth muscle actin (SMA) and transgelin (SM22) expression in control VSMC-like cells showed the presence of both proteins in all controls after transdifferentiation (Fig. 1B). Quantification of SMA and SM22 protein levels also revealed variability in expression between the controls. The variability in relative protein expression of SMA in the controls ranged from 0.46 to 1.54 (Fig. 1C) and 0.54 to 1.4 for SM22 (Fig. 1D). Western blot analysis was performed to demonstrate baseline values for control fibroblasts (Supplementary Material, Fig. S5).

Subsequently, we determined the transdifferentiation efficiency by analyzing the protein expression level of SMA and the organization of the newly expressed SMA fibers by immunofluorescence. Representative images are shown in Supplementary Material, Figure S1. Quantification of the immunofluorescent staining is shown in Supplementary Material, Figure S3. All cells were positive for both markers, although marker expression was variable. To quantify the amount of VSMC-specific SMA fibers, we determined the ratio between SMA fibers and total F-actin content in the cytoplasm. The transdifferentiated controls showed an overlay of ~30% of SMA fiber fluorescence with total F-actin, with the 2 × standard deviation (SD) range running from 0 to 61% (Fig. 1E). SMA fibers anisotropy, as an indicator of fiber organization, was quantified. Control VSMC-like cells showed a mean anisotropy coefficient of 0.25, with a range from 0.07 to 0.43 (Fig. 1F).

Taken together, these data show that all controls can be transdifferentiated to VSMC-like cells upon stimulation with TGF$\beta$, as confirmed by SMA and SM22 marker expression and SMA fiber organization.

### Transdifferentiation efficiency of VSMC-like cells of aneurysm patients

The goal of our study is to develop functional assays to determine aberrant phenotypes in AA patient cells. Since these assays have not been previously used to uncover the consequences of the mutations on VSMC function, there is no quantitative reference available for normal cell output. We thus used the mean and 2 × SD range of the control cell lines as a reference and compared the output of patient cells to determine if they were considered significantly aberrant from the range of the controls.

Transdifferentiation efficiency was determined by quantitative western blot analysis of SMA and SM22 protein levels (Fig. 2A). SMA and SM22 were present after transdifferentiation in both cell lines with a mutation in cytoskeleton encoding genes. Quantification revealed increased SMA protein levels (1.59) in ***ACTA2* #1** VSMC-like cells (Fig. 2B, $P < 0.01$), whereas SM22 protein levels (1.03) were comparable with controls (Fig. 2C). ***MYH11* #1** VSMC-like cells showed increased SMA protein levels (1.37) compared with controls, suggesting increased transdifferentiation potential (Fig. 2B, $P < 0.05$). SM22 was significantly decreased (0.69) in ***MYH11* #1** VSMC-like cells compared with controls, but was also remained in the control range (Fig. 2C, $P < 0.05$). SMA was almost undetectable (0.08) in ***SMAD3* #1** VSMC-like cells compared with controls, and SM22 protein levels (0.51) were decreased (Fig. 2B and C, $P < 0.001$). ***FBN1* #1 *HI*** and ***FBN1* #2 *HI*** VSMC-like cells showed similar SMA (0.92 and 1.47, respectively) and SM22 (0.94 and 0.95, respectively) protein levels to controls after transdifferentiation (Fig. 2B and C). ***FBN1* #3 *DN*** VSMC-like cells showed decreased SMA protein levels (0.39) compared with controls (Fig. 2B, $P < 0.01$), whereas having comparable SM22 protein levels (1.06) (Fig. 2C).

Transdifferentiation efficiency was further assessed by immunofluorescence (representative images are shown in Supplementary Material, Figure S2). Quantification of the immunofluorescent staining is shown in Supplementary Material, Figure S3. Baseline values for all non-transdifferentiated control and patient fibroblast are quantified and shown in Supplementary Material, Figure S4. Quantification of SMA fiber fluorescence, normalized for total F-actin, showed that ***ACTA2* #1** and ***MYH11* #1** VSMC-like cells have a similar SMA fluorescence as controls, 30 and 29%, respectively (Fig. 2D). Analysis of anisotropy confirmed decreased organization of SMA (0.099) in ***ACTA2* #1** VSMC-like cells (Fig. 2E, $P < 0.001$). ***MYH11* #1** VSMC-like cells showed a similar anisotropy for SMA (0.23) as controls (Fig. 2E). Quantification of SMA fluorescence levels revealed that SMA fluorescence levels (6.5%) were significantly reduced in ***SMAD3* #1** VSMC-like cells (Fig. 2D, $P < 0.001$). SMA fibers that were present in ***SMAD3* #1** VSMC-like cells after TGF$\beta$ stimulation furthermore showed a significantly decreased SMA anisotropy (0.12) compared with controls (Fig. 2E, $P < 0.01$). ***FBN1* #1 *HI*** and ***FBN1* #2 *HI*** VSMC-like cells showed similar SMA fluorescence, 22 and 26%, respectively, compared with controls (Fig. 2D). Quantification of anisotropy for SMA (0.22 and 0.30) in ***FBN1* #1 *HI*** and ***FBN1* #2 *HI*** VSMC-like cells revealed no aberrations in the fiber organization compared with controls (Fig. 2E). In contrast, after stimulation with TGF$\beta$ DN ***FBN1* #3 *DN*** VSMC-like cells showed a very low presence of SMA-positive cells with a significant decrease in intensity in SMA fluorescence (8.9%), suggesting transdifferentiation potential (Fig. 2D, $P < 0.001$). The SMA fibers in ***FBN1* #3 *DN*** VSMC-like cells showed no aberrations in SMA anisotropy (0.20) compared with controls (Fig. 2E).

In conclusion, SMA and SM22 western blot and immunostaining indicated that ***SMAD3* #1** and ***FBN1* #3 *DN*** cells did not develop SMA fibers and have a decreased transdifferentiation potential. ***ACTA2* #1** VSMC-like cells showed disorganized SMA fibers.

### Kinetics of pSMAD2 activation in control and AA patients' fibroblasts

To investigate the effects of TGF$\beta$ stimulation over time on TGF$\beta$ signaling activity, the C-terminal phosphorylation of SMAD2

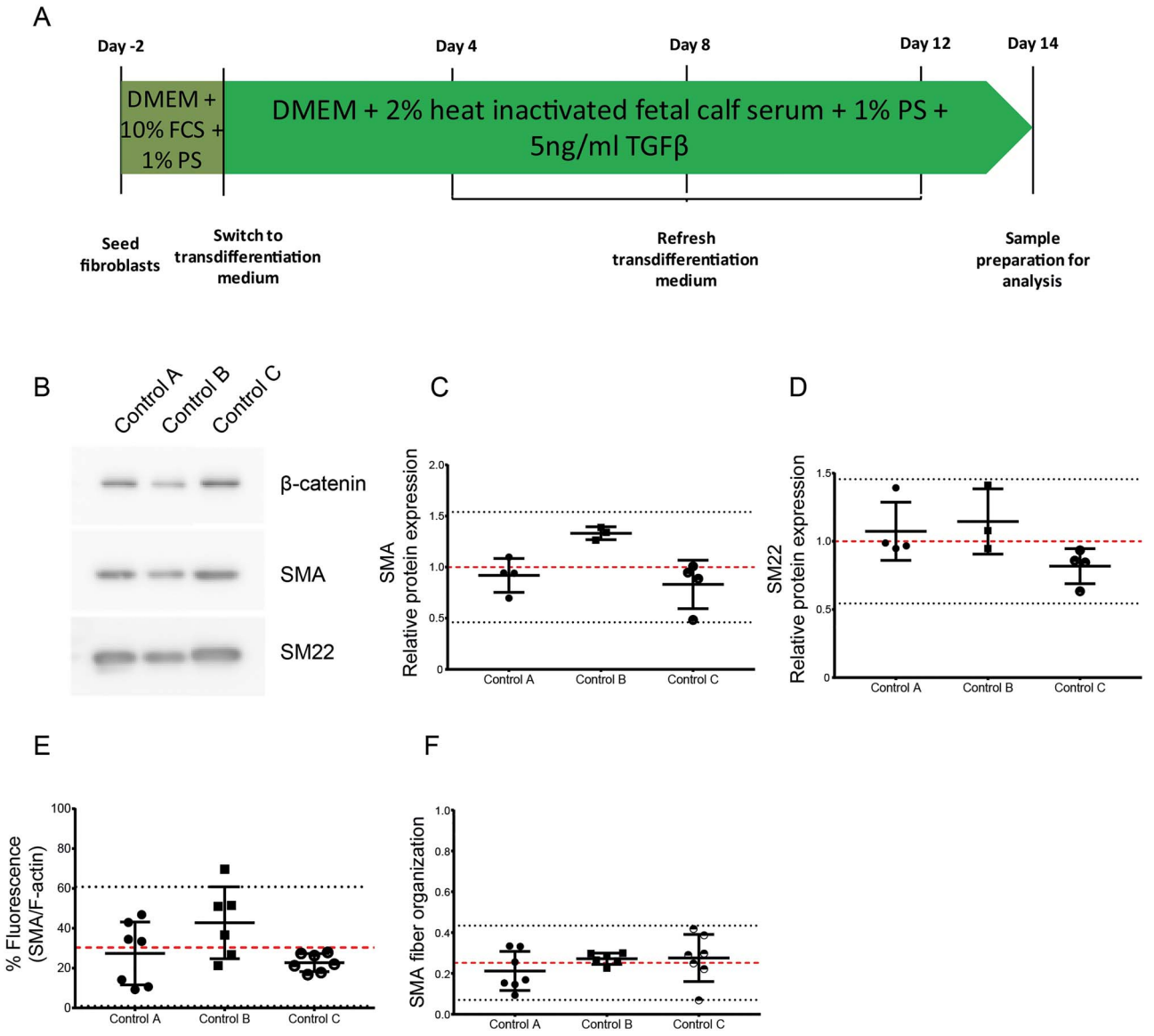


**Figure 1.** Baseline values for control VSMC-like cell transdifferentiation efficiency. (**A**) Schematic representation of the transdifferentiation protocol. (**B**) Western blot detecting SMA and SM22 protein expression and $\beta$-catenin expression as loading control. (**C**) Quantification of western blot SMA normalized by $\beta$-catenin expression. (**D**) Quantification of western blot SMA normalized by $\beta$-catenin expression. Each data point represents a separate experiment, $n = 3$. (**E**) Quantification of immunofluorescent staining for SMA, normalized by total F-actin fluorescence. (**F**) SMA fiber anisotropy. Each data point represents a separate image, $n = 7$. Data are presented as boxplots with mean $\pm$ 2SD; red dotted line indicates mean value, black dotted lines indicate $\pm$2SD.

was analyzed, as illustrated in Figure 3A. The response of non-transdifferentiated control fibroblasts to TGF$\beta$ over time was calculated from the ratio of receptor-activated (phosphorylated) SMAD2 compared with total SMAD2 protein following TGF$\beta$ stimulation (Fig. 3B). Overall, phosphorylated SMAD2 was detected 15 min after stimulation with TGF$\beta$. The amount of phosphorylated SMAD2 peaked after 30 min in the controls and the expression level at this time point was used as a reference for TGF$\beta$ signaling activity. At the 30 min time point, the mean pSMAD2/SMAD2 ratio was ~1 and ranged from 0.32 to 1.72 (Fig. 3B).

TGF$\beta$ signaling activity in patient fibroblasts was compared with the ratio obtained from the mean and 2 $\times$ SD ratio of the controls. ***ACTA2* #1** fibroblasts showed a pSMAD2/SMAD2 ratio of 0.44 after 30 min of TGF$\beta$ stimulation, which was just above the 2 $\times$ SD range of the controls (Fig. 3C). ***MYH11* #1** fibroblasts showed comparable phosphorylation of SMAD2 to control fibroblasts (Fig. 3C). Quantification also indicated a normal pSMAD2/SMAD2 ratio of 0.98 for ***MYH11* #1** fibroblasts compared with controls (Fig. 3C). Phosphorylation of SMAD2 was comparable with controls for ***SMAD3* #1** fibroblasts, the pSMAD2/SMAD2 ratio at 30 min of 1.35 and was therefore similar to the controls (Fig. 3D). SMAD2 phosphorylation in ***FBN1* #1 *HI*** and ***FBN1* #2 *HI*** fibroblasts showed similar pSMAD2/SMAD2 ratios, 0.72 and 1.08, respectively, compared with controls after 30 min of TGF$\beta$ stimulation (Fig. 3E). ***FBN1* #3 *DN*** fibroblasts showed reduced phosphorylation of SMAD2 after TGF$\beta$ stimulation (Fig. 3E). The pSMAD2/SMAD2 ratio of 0.46 for ***FBN1* #3 *DN*** fibroblasts after 30 min of TGF$\beta$ stimulation remained just above the 2 $\times$ SD range of the controls (Fig. 3E).

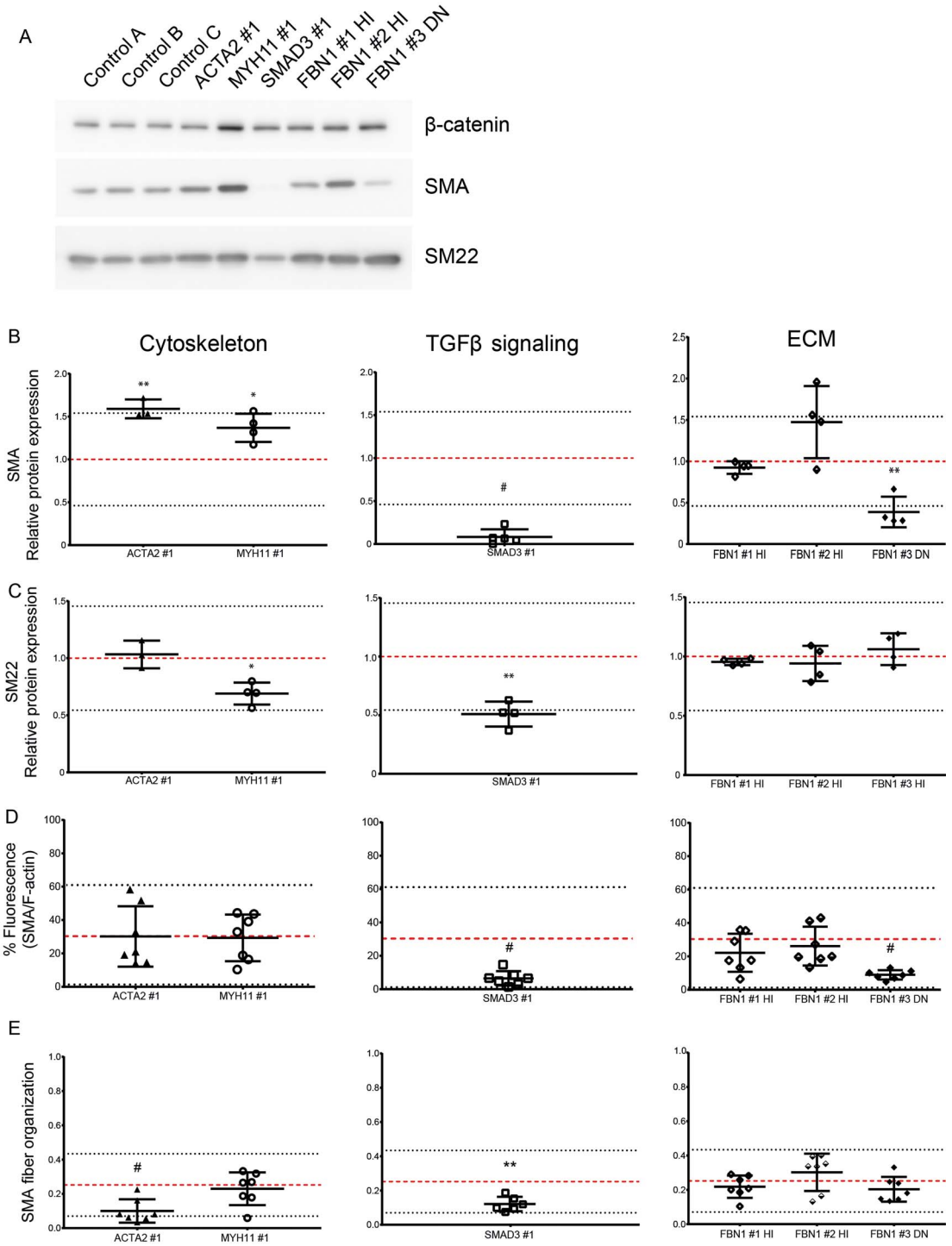


**Figure 2.** Transdifferentiation efficiency of VSMC-like cells of aneurysm patients with a pathogenic mutation. (**A**) Western blot detecting SMA and SM22 protein expression and $\beta$-catenin expression as loading control in three control cell and six patient VSMC-like cells. (**B**) Quantification of western blot SMA expression normalized by $\beta$-catenin expression. (**C**) Quantification of western blot SM22 expression normalized by $\beta$-catenin expression. Each data point represents a separate experiment, $n = 3$. (**D**) Quantification of immunofluorescent staining for SMA, normalized by total F-actin fluorescence. (**E**) SMA fiber anisotropy. Each data point represents a separate image, $n = 7$. Data are presented as boxplots with mean $\pm$ 2SD; red dotted line indicates mean value of the control cells, black dotted lines indicate $\pm$2SD.

Taken together, these data show that pSMAD2 activation is highly dynamic. In non-transdifferentiated cells, we detected differences in ***ACTA2 #1*** and ***FBN1 #3 DN*** cells compared with controls, although with considerable inter-experimental variability.

## Migration capacity of control and VSMC-like cells with a pathogenic variant

The migration capacity of the transdifferentiated VSMC-like cells was investigated with the use of a ring barrier migration

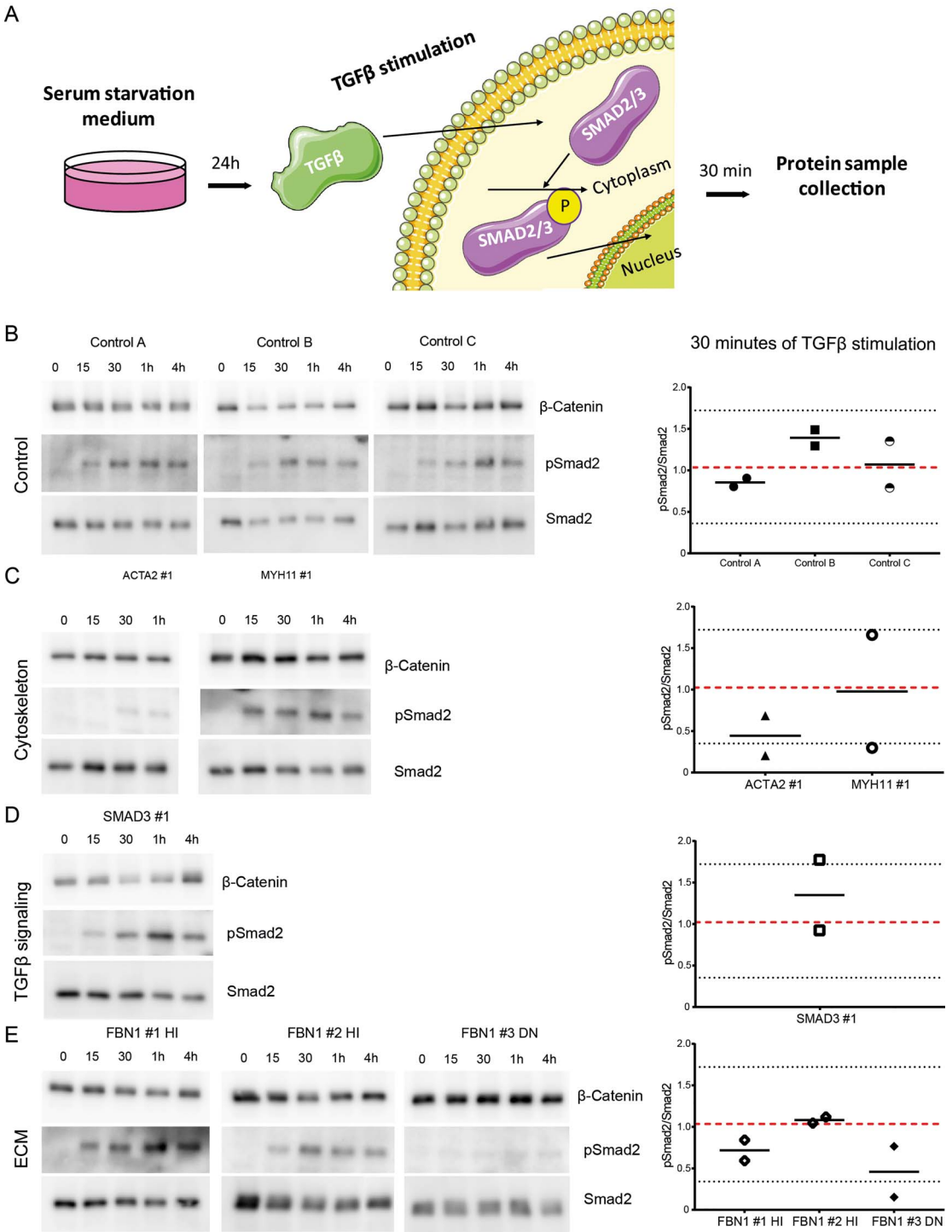


**Figure 3.** TGF$\beta$ responsiveness of control and fibroblasts of patients with a pathogenic mutation. **(A)** Schematic depicting TGF$\beta$ stimulation of control and patient fibroblasts. Cells are serum starved for 24 h, upon which they are stimulated with TGF$\beta$, which induces SMAD2 phosphorylation. Samples are harvested for western blot after 30 min. **(B)** Western blots detecting pSMAD2 and SMAD2 in control fibroblasts before and upon stimulation with TGF$\beta$ (15, 30 min, 1 and 4 h) and quantification of the pSMAD2/SMAD2 ratio. **(C)** Western blots detecting pSMAD2 and SMAD2 in fibroblasts with a mutation in a cytoskeleton encoding gene before and upon stimulation with TGF$\beta$ (15, 30 min, 1 and 4 h) and quantification of the pSMAD2/SMAD2 ratio. **(D)** Western blots detecting pSMAD2 and SMAD2 in fibroblasts with a mutation in a TGF$\beta$ signaling pathway encoding gene before and upon stimulation with TGF$\beta$ (15, 30 min, 1 and 4 h) and quantification of the pSMAD2/SMAD2 ratio. **(E)** Western blots detecting pSMAD2 and SMAD2 in fibroblasts with a mutation in an ECM encoding gene before and upon stimulation with TGF$\beta$ (15, 30 min, 1 and 4 h) and quantification of the pSMAD2/SMAD2 ratio. $\beta$-catenin levels serve as a loading control. Data are presented as boxplots with mean $\pm$ 2SD; red dotted line indicates mean value of the control cells, black dotted lines indicate $\pm$2SD.

**Table 1.** Information on cell line numbers, genes, transcript numbers, pathogenic variants and expected effects on the affected protein in patient cell lines

| Gene | Cell line | Pathogenic variant | Expected effect on protein | Cellular process |
|---|---|---|---|---|
| *ACTA2* (NM_001613.3) | **ACTA2 #1** | c.445C > T, p.R149C | Missense mutation, presumably affecting the fiber formation due to the disappearance of a positive amino acid load | Cytoskeleton contractility |
| *MYH11* (NM_002474.3) | **MYH11 #1** | c.3879 + 2dup, p.? | Splice site mutation, premature stop codon. Possibly leading to haploinsufficiency and absence of functional protein | Cytoskeleton contractility |
| *SMAD3* (NM_005902.3) | **SMAD3 #1** | c.859C > T, p.R287W | Missense mutation, potential loss of H-bridges at interacting site that leads to reduced SMAD3/SMAD4 complex stability | TGF$\beta$ signaling |
| *FBN1* (NM_000138.4) | **FBN1 #1 HI** | c.2369insC, p.C790Sfs*12 | Frameshift, premature stop codon resulting in haploinsufficiency | Extracellular matrix organization |
| | **FBN1 #2 HI** | c.2851insG, p.L951Afs*2 | Frameshift, premature stop codon resulting in haploinsufficiency | Extracellular matrix organization |
| | **FBN1 #3 DN** | c.2132G > A, p.C711Y | Missense mutation in the TGF$\beta$-binding protein-like domain that could affect binding to fibrillin-1 and results in a dominant negative effect on the protein | Extracellular matrix organization |

assay (Fig. 4A). Migration velocity of ***ACTA2 #1*** VSMC-like cells was decreased (5.0 versus 9.0 µm/h in controls) ($P < 0.001$, Fig. 4B). Likewise, ***MYH11 #1*** VSMC-like cells showed decreased migration velocity (3.5 versus 9.4 µm/h in controls) ($P < 0.001$, Fig. 4C). ***SMAD3 #1***, ***FBN1 #1 HI and #3 DN*** VSMC-like cells showed similar migration velocity as controls (Fig. 4D–F).

These data indicate that the migration assay was informative for ***ACTA2 #1*** and ***MYH11 #1*** VSMC-like cells, showing reduced migration after transdifferentiation.

### Contractility of pathogenic variant and control VSMC-like cells

Contractility of VSMC-like cells was determined upon ionomycin stimulation using the electric cell-substrate impedance sensing (ECIS) (Fig. 5A). The maximum contraction of control VSMC-like cells was on average 49.7% with a 2 × SD ranging from 23.3 to 76.1% (Fig. 5B). The maximum contraction of ***ACTA2 #1*** VSMC-like cells was 16.3% and thereby below the 2 × SD range of the controls. ***MYH11 #1*** VSMC-like cells showed a maximum contraction of 42.1% and did not differ from controls (Fig. 5C). ***SMAD3 #1*** VSMC-like cells displayed a maximum contraction of 70.4%, indicating a slight, but not significant, increase in contractility (Fig. 5D). ***FBN1 #1 HI*** and ***FBN1 #2 HI*** VSMC-like cells had a maximum contractility of 47.8 and 47.2%, respectively, and were thereby comparable with the controls. Likewise ***FBN1 #3 DN*** VSMC-like cells were similar to controls with a maximum contraction of 46.5% (Fig. 5E).

From these data, we can conclude that the contractility assay was informative for ***ACTA2 #1*** VSMC-like cells showing a reduced contractility. In the other patients, contractility was unimpaired.

## Discussion

Genetic causes for syndromal and non-syndromal AA include a growing number of variants in genes with a wide range of interacting functions. It is important to find ways to distinguish and quantify the detrimental effects of variants in these genes into pathogenic and non-pathogenic, in particular due to the wide implementation of next-generation sequencing for molecular diagnosis of genetic aneurysms and *in vitro* classification of variants, resulting in a growing number of VUS. Functional assays with robust readouts for pathogenic effect will help to improve the diagnostic yield of aneurysm testing.

In this study, we used VSMC-like cells of AA patients to evaluate the clinical relevance of novel functional assays that could detect the pathologic molecular phenotype and measure the effect of different pathogenic variants in aneurysm-related genes. We measured a strong decrease in SMA expression and thereby reduced transdifferentiation potential in *SMAD3* and *FBN1* dominant negative (*FBN1* #3 DN) patient cells. *ACTA2* and *FBN1* DN patients also showed a decrease in intracellular TGF$\beta$ signaling. Migration velocity was impaired for *ACTA2* and *MYH11*, whereas only *ACTA2* showed reduced contractility. Below, we will discuss these results per mutation. A summary of the data can also be found in Table 2. VMCs can uniquely be distinguished by the expression of VSMC-specific markers, such as SMA, calponin, SM22 and MYH11. As we demonstrated in our previous publication (31) where we first described and validated the method, our cells phenocopy VSMCs as they express calponin and smoothelin on protein level, markers of mature contractile SMC. We also demonstrated that in VSMC-like cells of AA patients, there is a significant upregulation of ACTA2, CNN1, MYH11, TAGLN and SMTN compared with non-transdifferentiated skin fibroblasts. As it was recently reported (32), smooth muscle myosin heavy chain, in combination with SMA is part of the cluster of markers, which allows discrimination between contractile and non-contractile cells, and calponin and smoothelin are auxiliary molecules of the contractile apparatus. Even though these markers are also presented in some myofibroblastic classes, the broad expression palette of VSMC markers in our cells indicates that they are close to VSMC. Based on previously published work by our groups, we chose SMA and SM22 as the two markers most technically reliable stable for both immunofluorescence and western blot to assess the transdifferentiation efficiency, to minimize any variability in experimental results that does not derive from the differences between control and patient cells (31).

### ACTA2

ACTA2 #1 VSMC-like cells demonstrated similar transdifferentiation potential as controls. However, their new SMA fibers, encoded by *ACTA2*, appeared fragmented and disorganized.

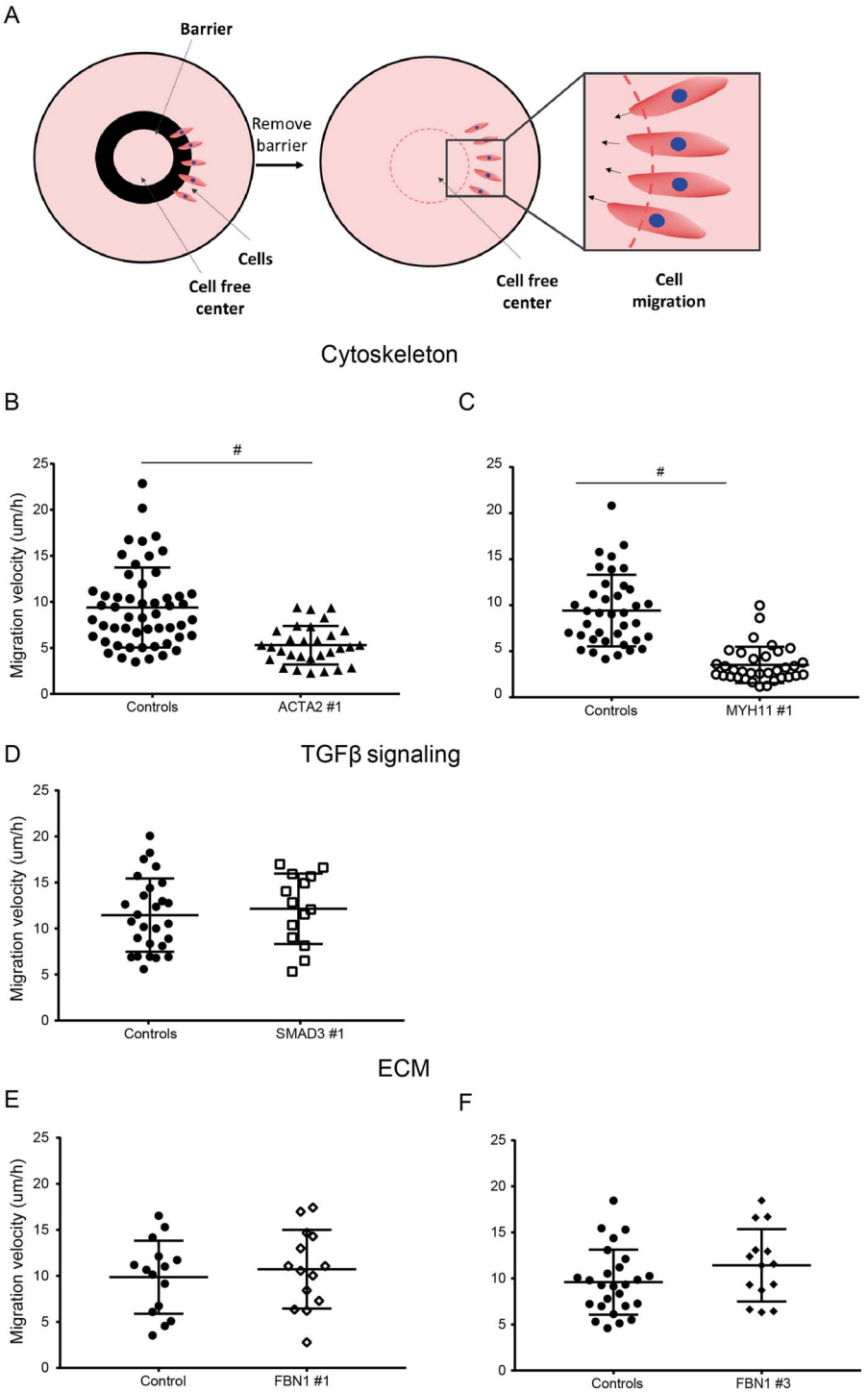


**Figure 4.** Migration potential of control and VSMC-like cells of patients with a pathogenic mutation. (**A**) Schematic representation of the ring barrier assay to measure migration. Cells are seeded on coverslips in the outside area of the wall. A ring is blocking the migration of the cells, preserving a cell-free are in the center. Once the ring is removed, cells start to migrate towards the center and the migration velocity is quantified. (**B**–**F**) Migration velocity of pathogenic variant VSMC-like cells compared with controls. (A) ACTA2, (B) MYH11, (C) SMAD3, (D) FBN1 #1 and (E) FBN1 #3 VSMC-like cells, $n = 2$, $^{\#}$ $P = <0.001$. Data are presented as boxplots with mean ± 2SD; red dotted line indicates mean value of the control cells, black dotted lines indicate ±2SD.

Guo *et al.* (4) previously showed lack of SMA fibers in VSMCs of patient with *ACTA2* variants (p.R118Q and p.T353N). Our data showed that the p.R149C variant of ACTA2 #1 resembles other known *ACTA2* pathogenic variants with its disorganized SMA fibers after transdifferentiation. Clinical data on *ACTA2* p.R149C, p.R256H and p.T353N aortic sections confirmed that SMA protein is produced, but that VSMCs appear to be disorganized and lack structure (33). Complications with the assembly of mutant SMA (p.R256H) is further confirmed by analysis of mutant *ACTA2* in yeast (33). Analysis of SMA fiber assembly by Malloy *et al.* (33)

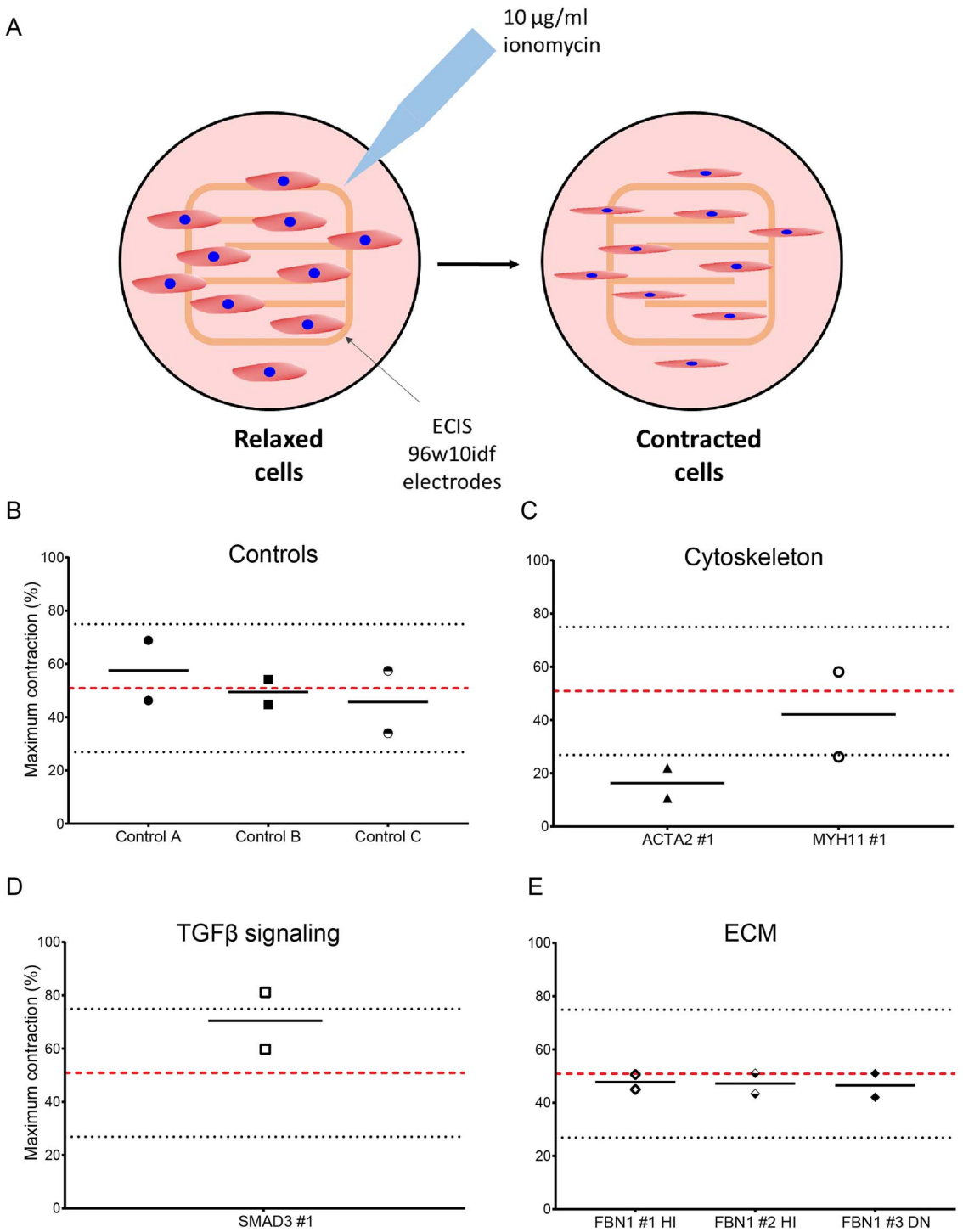


**Figure 5.** Maximum contraction of control and VSMC-like cells of patients with a pathogenic mutation. (**A**) Schematic representation of measuring VSMC-like cell contractility using ECIS. Cells are seeded on electrodes which record the baseline resistance of relaxed cells as a function of their surface. Upon ionomycin stimulation, cells contract, which reduces their surface and subsequently resistance. (A) Maximum contraction of controls VSMC-like cells. (**B**) Maximum contraction of ACTA2 and MYH11 variant VSMC-like cells. (**C**) Maximum contraction of SMAD3 variant VSMC-like cells. (**D**) Maximum contraction of FBN1 variant VSMC-like cells, $n = 2$. Data are presented as boxplots with mean ± 2SD; red dotted line indicates mean value of the control cells, black dotted lines indicate ±2SD.

showed decreased SMA polymerization and elongated assembly times in *ACTA2* p.R256H mutant yeast compared with wild-type yeast. Studies on *ACTA2* pathogenic variants (p.R118Q, p.R256H and p.T353N) show overall disorganization of SMA fibers that is caused by dysfunctional assembly of SMA. Our results confirmed elucidated the disorganization of SMA for an additional *ACTA2* pathogenic variant (p.R149C) in VSMC-like cells.

In addition, ACTA2 #1 VSMC-like cells showed decreased migration and contractility. During migration, the cytoskeleton is polymerized in the direction of movement, whereas depolymerization occurs at the rear end of cells. Variants in proteins

that constitute the cytoskeleton, such as *ACTA2* and *MYH11*, can be explanatory for the observed defective migration. Literature revealed that *ACTA2* is induced during migration as well as during metastasis, suggesting that *ACTA2* is essential for migration (34,35). Decreased contractility of multiple *ACTA2* pathogenic variant VSMCs was previously found by Lu *et al.* (36) by performing a one-bead laser trap experiment to analyze force output. Our data on the reduced contractility of ACTA2 #1 VSMC-like cells is in line with this finding and highlights importance of *ACTA2* for the contractility of VSMCs.

### MYH11

MYH11 #1 VSMC-like cells showed decreased SM22 protein levels post transdifferentiation. Overexpression of *MYH11* has been reported to induce degradation and turnover of thick filament-associated proteins and cytoskeleton proteins like SM22 but not SMA (37). Since *MYH11* c.3879 + 2dup (MYH11 #1) is a relatively unknown variant, it is unclear whether this variant could lead to reduced levels or function of *MYH11*. Our finding that SMA is not degraded is in line with the results of Kwartler *et al.* (37) and suggests that this *MYH11* pathogenic variant could indeed induce the described unfolded protein response that induces degradation of specific cytoskeleton proteins. Although the MYH11 #1 VSMC-like cells were able to transdifferentiate, migration velocity was decreased in *MYH11* variant VSMC-like cells, similar to the ACTA2 #1 VSMC-like cells. *MYH11* pathogenic variants have been predicted to compromise SMC migration, which is in line with our results (38,39).

### SMAD3

SMAD3 #1 VSMC-like cells did not develop SMA fibers upon transdifferentiation, suggesting reduced transdifferentiation potential. This lack of SMA could be explained by disturbance in the TGF$\beta$ signaling pathway caused by the *SMAD3* pathogenic variant. Induction of SMA by TGF$\beta$ was shown to occur via *SMAD3* (40,41), suggesting that induction will not occur when *SMAD3* is mutated. Like SMA, SM22 is induced via activation of the TGF$\beta$ pathway, specifically via *SMAD3* (42). This also explains the reduced SM22 protein levels of *SMAD3* pathogenic variant VSMC-like cells. The TGF$\beta$ signaling pathway is often considered physiologically active when SMAD2 is phosphorylated upon TGF$\beta$ stimulation, yet, for *SMAD3* variants resulting in absent or defective SMAD3 proteins, this is not necessarily true (43). Although, the initial response to TGF$\beta$ stimulation is intact in *SMAD3* knockout cells, downstream signaling is impaired due to absence of SMAD3 protein. This hampers induction of target genes, thereby leading to impaired induction of SMA and SM22 and thus diminished transdifferentiation.

### FBN1

VSMC-like cells with a *FBN1* DN pathogenic variant (FBN1 #3) express less SMA protein as wells as SMA fibers after transdifferentiation. This could be caused by defective ECM build-up resulting from the *FBN1* variant, resulting in reduced binding sites for the cytoskeleton via integrins. The rigidity of the ECM is also important for the development of the cytoskeleton as, for example, a soft matrix results in a less well-defined cytoskeleton (44–46). The effect of a defective matrix on the cytoskeleton has recently also been shown in the *Fibulin*-4 VSMC-specific knockout mouse model in which absence of fibulin-4 led to absence of SMA protein and fibers (47).

Transdifferentiation of *FBN1* DN and HI patient fibroblasts reveals differential results between two (predicted) types of *FBN1* pathogenic variants. Although the DN FBN1 #3 VSMC-like cells show decreased induction of SMA and SM22, results from FBN1 #1 and #2 HI fibroblasts appear quite similar to controls. Clinical data have previously also suggested differences between the *FBN1* DN and HI variant in their responsiveness to treatment with losartan (48,49). Patients with an *FBN1* HI pathogenic variant that received treatment with losartan were responsive to the inhibition of aortic root dilation by losartan, whereas *FBN1* DN patients did not respond to treatment (48). Furthermore, patients with an *FBN1* HI variant showed improvement in biventricular end diastolic volume and stroke volume upon losartan treatment. This effect was not found in *FBN1* DN patients that received losartan (49). This indicates that pathogenic variants in one gene can lead to different outcomes and could result in different clinical consequences for patients, which is in line with the nature of the *FBN1* variants and their effects. HI variants result in half of the normal protein levels, whereas DN variants interfere with the normal protein and can result in non-functional protein levels. Our functional assays proved to be able to identify characteristics potentially distinguishing between *FBN1* HI and DN pathogenic variants. Their application could potentially simplify the identification of HI and DN patients. Especially, the presence or absence of SMA, and potentially the pSMAD2/SMAD2 ratio, after TGF$\beta$ stimulation can distinguish *FBN1* DN VSMC-like cells from *FBN1* HI VSMC-like cells.

A possible limitation of our study is that only one cell line was used per pathogenic variant. We chose to analyze a set of pathogenic variants in the more frequently affected aneurysm genes and validate assays for assessing the roles of the pathogenic variant on RNA and protein expression and function. However, rather than drawing strong conclusions about each mutation, we wanted to demonstrate that these assays can be used to study the functional aspects of a wider range of mutations involved in AA pathogenesis. We plan to perform larger scale analysis in the future, with multiple cell lines of different pathogenicity, to use our assays to study the mechanistics of these mutations.

## Conclusion

The assays which were tested showed promising applicability for distinguishing effects of pathogenic variants in the selected genes. We detected reduced transdifferentiation potential was noted in **SMAD3 #1** and **FBN1 #3 DN**, defective migration in **MYH11 #1** and **ACTA2 #1** and defective contractility in **ACTA2 #1**. Further testing of pathogenic variants in these and other genes is needed to establish a panel of assays that can be used for testing effects of those variants. Our results suggest a potential application for these novel functional assays in assessing the functionality of a larger number of proteins encoded by the same genes. Hopefully, this will result in the ability to analyze the potential pathogenic effect of VUS in AA genes and thereby promote more accurate genetic diagnosis and family counseling for AA.

## Materials and Methods

### Cell lines and patient characteristics

Primary dermal fibroblasts of AA patients and controls were obtained from the biobanks of the departments of Clinical Genetics (Amsterdam University Medical Center—location

**Table 2.** Summary of findings

| | Transdifferentiation potential | | | | TGF$\beta$ responsiveness | Cytoskeleton function | |
|---|---|---|---|---|---|---|---|
| | Immunofluorescence | | Western blotting | | pSMAD2/SMAD2 ratio (30 min) | Migration | Contractility |
| | % SMA | SMA organization | SMA | SM22 | | | |
| Pathogenic Variant | Versus controls | Versus controls | Versus controls | Versus controls | Versus controls | Versus controls | Versus controls |
| ACTA2 #1 | ~ | ↓* | ↑ | ~ | ↓ | ↓ | ↓ |
| MYH11 #1 | ~ | ~ | ↑* | ↓* | ~ | ↓ | ~ |
| SMAD3 #1 | ↓ | ↓* | ↓ | ↓ | ~ | ~ | ~ |
| FBN1 #1 HI | ~ | ~ | ~ | ~ | ~ | ~ | ~ |
| FBN1 #2 HI | ~ | ~ | ~ | ~ | ~ | - | ~ |
| FBN1 #3 DN | ↓ | ~ | ↓ | ~ | ↓ | ~ | ~ |

~= no difference; ↓ = trend of decrease; ↓* = significantly decreased; ↑ = trend of increase; ↑* = significantly increased.

VUmc and Erasmus University Medical Center, The Netherlands) for all experiments. Fibroblasts were cultured in Dulbecco's-modified Eagle's medium (DMEM, Lonza BioWhittaker) supplemented with 10% fetal calf serum (FCS) and 1% penicillin/streptomycin (PS) at 37°C with 5% $CO_2$. Fibroblasts of healthy controls and AA patients with heterozygous mutations in *ACTA2* (cytoskeleton), *MYH11* (cytoskeleton), *SMAD3* (TGF$\beta$ signaling) and *FBN1* (ECM) were used for all experiments (see Table 1 for genotypes of pathogenic variants). The pathogenic variants were evaluated by the Alamut Visual, a decision-support software for genome variant diagnostics, and were classified according to American College of Medical Genetics and Genomics (ACMG) as class 5.

## Transdifferentiation protocol

Fibroblasts were seeded at a density of 2.5 million cells/ml as previously described (31). Fibroblasts were seeded in DMEM with 10% FCS and 1% PS at a density of 2.5 million cells/ml on the corners of a 1 $cm^2$ piece of Matriderm (MedSkin Solutions), meaning 250 000 cells per piece of Matriderm. Two days after seeding, the medium was changed to DMEM supplemented with 2% heat-inactivated FCS, 1% PS and 5 ng/ml human recombinant TGF$\beta$1 (4342-5, BioVision). Heat inactivation was performed by placing the FCS in a 56°C water bath for 30 min and mixing regularly. Medium supplemented with TGF$\beta$1 was changed every 4 days. After 14 days, the cells were enzymatically extracted from the Matriderm with the use of a collagenase solution in complete medium (2000 IU/ml, Worthington) at 37°C on a shaker for 3 h. Centrifugation was performed to remove collagenase and cells were transferred to new flasks and cultured for further experiments. Passage number of 'VSMC-like' cells after transdifferentiation was kept below five to prevent loss of transdifferentiation markers.

## Immunofluorescent staining and image quantification

Dermal fibroblasts were seeded on 18 mm coverslips in 12-well plates with a density of 100 000 cells/well in DMEM with 10% FCS and 1%PS. Two days after seeding, the medium was changed to DMEM supplemented with 2% heat-inactivated FCS, 1% PS and 5 ng/ml human recombinant TGF$\beta$1 (4342-5, BioVision). TGF$\beta$ supplemented medium was changed every 4 days, and after 14 days, cells were fixed with 2% paraformaldehyde in phosphate-buffered saline (PBS) for 15 min. After fixation, cells were washed with PBS supplemented with 0.1% Triton X-100 and blocked with PBS+ (0.5% bovine serum albumine (BSA) and 0.15% glycine in PBS) for 30 min. Primary antibodies were incubated overnight at 4°C in PBS+; mouse monoclonal anti-SMA (1:1000, ab7817, Abcam) and rabbit polyclonal anti-SM22 (1:400, ab14106, Abcam). Cells were washed with PBS supplemented with Triton X-100 and incubated shortly with PBS+ prior to incubation with the secondary antibody in PBS+ (1:1000, anti-mouse Alexa Fluor 488 and anti-rabbit Alexa Fluor 594, Molecular Probes) for 1 h at room temperature. Simultaneously, actin filaments were stained with SiR-Actin (1:1000, Cytoskeleton). After incubation, coverslips were mounted on glass slides with Vectashield supplemented with 4′,6-diamidino-2-phenylindole (DAPI) (H-1200, Vector Laboratories) and sealed with nail polish. Images were recorded on a wide field epifluorescent microscope (Axio Imager D2, Zeiss).

Quantification of the immunofluorescent signal was performed by calculating the corrected total cell fluorescence (CTCF) of SMA and actin. The CTCF of actin and SMA was determined by setting a color threshold to select the fibers in the image with Fiji image analyzing software (50) and determining the integrated density of this area (intensity of the fluorescence). This measurement was corrected for the background fluorescence and the total area of the fibers and results in the CTCF. The percentage of fluorescence was calculated by dividing SMA CTCF by total F-actin CTCF to determine what percentage of the actin cytoskeleton is positive for SMA compared with the total actin cytoskeleton [Eq. (1)].

$$\%\ \text{Fluorescence} = \frac{\text{SMA CTCF}}{\text{F} - \text{actin CTCF}} \quad (1)$$

Equation 1: Percentage of fluorescence.

Cytoskeletal fiber organization was assessed by measuring anisotropy on microscopic images using FibrilTool plug-in in Fiji (51). The anisotropy coefficient ranges from zero to one; parallel lines result in an anisotropy coefficient of one, whereas non-parallel structures have an anisotropy coefficient close to zero. The alignment of SMA fibers was assessed in confocal images of transdifferentiated cells of controls and patients with a pathogenic variant. According to the published protocol, X–Y

fields of view were marked as regions of interest, and anisotropy was quantified within those regions.

### Western blotting

VSMC-like cells were seeded at 100000 cells/six-well and allowed to attach for 48 h. Cells were scraped in PBS supplemented with protease inhibitor cocktail (1:100, 11836145001, Roche Applied Science) and phosphatase inhibitor cocktail (1:100, P0044, Sigma) and lysed in equal volumes of 2× Laemmli buffer (4% SDS, 20% glycerol, 120 mM Tris pH 6.8) supplemented with protease inhibitor cocktail and phosphatase inhibitor. Lysates were cleared of large DNA by passing through a 25G needle and then heated to 65°C for 10 min. Protein concentrations were measured with the Lowry protein assay (52). Equal amounts of protein were size separated by SDS-PAGE and separated proteins were then transferred to a polyvinylidene difluoride (PVDF) membrane (1 h, 100 V, Immobilon). Membranes were blocked for 1 h at room temperature by either 5% BSA or 3% milk in PBS supplemented with 0.1% Tween-20. Membranes were incubated 45 min at room temperature with primary antibody. Membranes were washed five times with 0.1% Tween-20 in PBS and then incubated with horseradish peroxidase-conjugated secondary antibodies (1:2000, Jackson ImmunoResearch) for 1 h at room temperature. Bound secondary antibodies were detected with an Amersham Imager 600 (GE Healthcare Life Sciences) using chemiluminescence. Band intensity was quantified using Fiji image analyzing software (50).

### Stimulation with TGF$\beta$

To investigate potential differences in sensitivity to TGF$\beta$ stimulation between control and patient fibroblasts, cells were seeded in DMEM supplemented with 10% FCS and 1% PS in six-well plates to reach confluence and were allowed to attach for 24 h. The following day, medium was changed to DMEM supplemented with 1% PS and fibroblasts were serum deprived for 24 h prior to stimulation with human recombinant TGF$\beta$. Protein samples were collected after 0, 15, 30 min, 1 and 4 h of stimulation with TGF$\beta$1 in a concentration of 5 ng/ml (4342-5, BioVision). Lysis of cells and western blotting was performed as described above. Membranes were incubated overnight at 4°C with primary antibody. The TGF$\beta$ responsiveness of the control fibroblasts was used to establish baseline values to compare responsiveness values of patient cell lines: values outside the mean $\pm 2 \times$ SD of the response in controls were considered abnormal.

### Ring barrier migration assay

To measure the migration speed, a ring barrier migration assay was performed (53). In this assay, a barrier is placed in a cell culture chamber that prevents cells from entering the cell-free area. VSMC-like cells are seeded outside of this barrier and form a monolayer prior to the removal of the barrier. Upon removal of the barrier, VSMC-like cells can migrate into the cell-free area and migration can be monitored. Migration speed can be deducted. Migration velocity can be calculated based on total migration and the duration of the experiment. A total of 50 000 VSMC-like cells were seeded in the outer ring of the set-up and were allowed to attach for 24 h. After removing the ring barrier, cells were washed twice with DMEM supplemented with 1% PS (serum free) and were left in this medium during migration to prevent cell division. Multiple locations at the migration front were selected to monitor movement. Every 10 min, pictures were taken at the selected locations for 24 h. Data were analyzed with the AxioVision software (version 4.5.0.0) by measuring the total migration length of multiple cells and calculating the migration velocity. The migration velocity of the controls was used to establish baseline for the measurements in the patient cell lines: values outside the mean $\pm 2 \times$ SD of the response were considered abnormal.

### Measuring cell contractility

Cell contractility was measured and calculated according to previously published protocol using the ECIS (54). VSMC-like cells were seeded in duplicate in the array at a density of 30 000 cells/well in a sterile 96-well plate array well (96w10; Ibidi, Planegg, Germany). Cells were cultured for 48 h prior to stimulation. The impedance was recorded at a frequency of 4000 Hz.

VSMC-like cells were stimulated with 10 µg ionomycin/ml (Sigma Aldrich, Darmstadt, Germany). Contractile responses were measured in duplicate in each experiment. Contraction (C) of each well equals one minus the ratio between the resistance post- (PoS) and pre- (PrS) stimulation post empty well value subtraction, as depicted in Eq. (2):

$$C = \left(1 - \frac{(\mathrm{PoS}\,[\Omega] - 290\,[\Omega])}{(\mathrm{PrS}\,[\Omega] - 290\,[\Omega])}\right) \bullet 100 \qquad (2)$$

Equation 2: Contractile response.

The maximum measured change in contraction was recorded and expressed as maximum contraction. To characterize the contractile output of patient fibroblasts, the mean response of the control group was used as a reference. Contraction of the patient VSMC-like cells was compared with a range between $2 \times$ SD above and below the mean contractile response of the control group.

### Statistics

Number of experiment replicates and independent samples are stated in the figure legends. Data were corrected for outliers with the Grubbs' test for outliers. Statistical analysis was performed with a non-parametric Mann–Whitney test. Significance was tested two-tailed against the mean of the controls. Significance in gene expression analysis of stimulated controls was tested two-tailed against unstimulated controls. A $P$-value $< 0.05$ was considered to indicate a significant difference between groups. In the figures, $P < 0.05$ is shown with $^{*}P < 0.01$ with $^{**}P < 0.001$ with $^{\#}$. Results are expressed as mean $\pm$ SD, real-time PCR results are expressed as mean $\pm$ SD. All analyses were performed using Graphpad, version 7.03.

## Supplementary Material

Supplementary Material is available at *HMG* online.

## Acknowledgements

The authors would like to thank Hanny Odijk for expert technical assistance.

*Conflict of Interest statement*. None declared.

## Funding

The authors would like to thank Stichting Lijf en Leven (Genexpressie analyse ter detective van de moleculaire mechanismen

van aneurysmavorming—GAMMA), Erasmus MC Mrace grant and Amsterdam Cardiovascular Sciences Institute (ICaR AiO 2015 PhD grant) for supporting this research.

## References


1. Kühnl, A., Erk, A., Trenner, M., Salvermoser, M., Schmid, V. and Eckstein, H.-H. (2017) Incidence, treatment and mortality in patients with abdominal aortic aneurysms: an analysis of hospital discharge data from 2005–2014. *Dtsch. Arztebl. Int.*, **114**, 391.
2. Ziganshin, B.A., Bailey, A.E., Coons, C., Dykas, D., Charilaou, P., Tanriverdi, L.H., Liu, L., Tranquilli, M., Bale, A.E. and Elefteriades, J.A. (2015) Routine genetic testing for thoracic aortic aneurysm and dissection in a clinical setting. *Ann. Thorac. Surg.*, **100**, 1604–1611.
3. van de Luijtgaarden, K.M., Heijsman, D., Maugeri, A., Weiss, M.M., Verhagen, H.J., IJpma, A., Bruggenwirth, H.T. and Majoor-Krakauer, D. (2015) First genetic analysis of aneurysm genes in familial and sporadic abdominal aortic aneurysm. *Hum. Genet.*, **134**, 881–893.
4. Guo, D.C., Pannu, H., Tran-Fadulu, V., Papke, C.L., Yu, R.K., Avidan, N., Bourgeois, S., Estrera, A.L., Safi, H.J., Sparks, E. *et al.* (2007) Mutations in smooth muscle alpha-actin (ACTA2) lead to thoracic aortic aneurysms and dissections. *Nat. Genet.*, **39**, 1488–1493.
5. Zhu, L., Vranckx, R., Khau Van Kien, P., Lalande, A., Boisset, N., Mathieu, F., Wegman, M., Glancy, L., Gasc, J.M., Brunotte, F. *et al.* (2006) Mutations in myosin heavy chain 11 cause a syndrome associating thoracic aortic aneurysm/aortic dissection and patent ductus arteriosus. *Nat. Genet.*, **38**, 343–349.
6. Wang, L., Guo, D.C., Cao, J., Gong, L., Kamm, K.E., Regalado, E., Li, L., Shete, S., He, W.Q., Zhu, M.S. *et al.* (2010) Mutations in myosin light chain kinase cause familial aortic dissections. *Am. J. Hum. Genet.*, **87**, 701–707.
7. Guo, D.C., Regalado, E., Casteel, D.E., Santos-Cortez, R.L., Gong, L., Kim, J.J., Dyack, S., Horne, S.G., Chang, G., Jondeau, G. *et al.* (2013) Recurrent gain-of-function mutation in PRKG1 causes thoracic aortic aneurysms and acute aortic dissections. *Am. J. Hum. Genet.*, **93**, 398–404.
8. Loeys, B.L., Chen, J., Neptune, E.R., Judge, D.P., Podowski, M., Holm, T., Meyers, J., Leitch, C.C., Katsanis, N., Sharifi, N. *et al.* (2005) A syndrome of altered cardiovascular, craniofacial, neurocognitive and skeletal development caused by mutations in TGFBR1 or TGFBR2. *Nat. Genet.*, **37**, 275–281.
9. Loeys, B.L., Schwarze, U., Holm, T., Callewaert, B.L., Thomas, G.H., Pannu, H., De Backer, J.F., Oswald, G.L., Symoens, S., Manouvrier, S. *et al.* (2006) Aneurysm syndromes caused by mutations in the TGF-beta receptor. *N. Engl. J. Med.*, **355**, 788–798.
10. Mizuguchi, T., Collod-Beroud, G., Akiyama, T., Abifadel, M., Harada, N., Morisaki, T., Allard, D., Varret, M., Claustres, M., Morisaki, H. *et al.* (2004) Heterozygous TGFBR2 mutations in Marfan syndrome. *Nat. Genet.*, **36**, 855–860.
11. Lindsay, M.E., Schepers, D., Bolar, N.A., Doyle, J.J., Gallo, E., Fert-Bober, J., Kempers, M.J., Fishman, E.K., Chen, Y., Myers, L. *et al.* (2012) Loss-of-function mutations in TGFB2 cause a syndromic presentation of thoracic aortic aneurysm. *Nat. Genet.*, **44**, 922–927.
12. Boileau, C., Guo, D.C., Hanna, N., Regalado, E.S., Detaint, D., Gong, L., Varret, M., Prakash, S.K., Li, A.H., d'Indy, H. *et al.* (2012) TGFB2 mutations cause familial thoracic aortic aneurysms and dissections associated with mild systemic features of Marfan syndrome. *Nat. Genet.*, **44**, 916–921.
13. Rienhoff, H.Y., Jr., Yeo, C.Y., Morissette, R., Khrebtukova, I., Melnick, J., Luo, S., Leng, N., Kim, Y.J., Schroth, G., Westwick, J. *et al.* (2013) A mutation in TGFB3 associated with a syndrome of low muscle mass, growth retardation, distal arthrogryposis and clinical features overlapping with Marfan and Loeys-Dietz syndrome. *Am. J. Med. Genet. A*, **161A**, 2040–2046.
14. Matyas, G., Naef, P., Tollens, M. and Oexle, K. (2014) De novo mutation of the latency-associated peptide domain of TGFB3 in a patient with overgrowth and Loeys-Dietz syndrome features. *Am. J. Med. Genet. A*, **164A**, 2141–2143.
15. Bertoli-Avella, A.M., Gillis, E., Morisaki, H., Verhagen, J.M.A., de Graaf, B.M., van de Beek, G., Gallo, E., Kruithof, B.P.T., Venselaar, H., Myers, L.A. *et al.* (2015) Mutations in a TGF-beta ligand, TGFB3, cause syndromic aortic aneurysms and dissections. *J. Am. Coll. Cardiol.*, **65**, 1324–1336.
16. van de Laar, I.M., Oldenburg, R.A., Pals, G., Roos-Hesselink, J.W., de Graaf, B.M., Verhagen, J.M., Hoedemaekers, Y.M., Willemsen, R., Severijnen, L.A., Venselaar, H. *et al.* (2011) Mutations in SMAD3 cause a syndromic form of aortic aneurysms and dissections with early-onset osteoarthritis. *Nat. Genet.*, **43**, 121–126.
17. van de Laar, I.M., van der Linde, D., Oei, E.H., Bos, P.K., Bessems, J.H., Bierma-Zeinstra, S.M., van Meer, B.L., Pals, G., Oldenburg, R.A., Bekkers, J.A. *et al.* (2012) Phenotypic spectrum of the SMAD3-related aneurysms-osteoarthritis syndrome. *J. Med. Genet.*, **49**, 47–57.
18. Dietz, H.C., Pyeritz, R.E., Hall, B.D., Cadle, R.G., Hamosh, A., Schwartz, J., Meyers, D.A. and Francomano, C.A. (1991) The Marfan syndrome locus: confirmation of assignment to chromosome 15 and identification of tightly linked markers at 15q15-q21.3. *Genomics*, **9**, 355–361.
19. Milewicz, D.M. (1994) Identification of defects in the fibrillin gene and protein in individuals with the Marfan syndrome and related disorders. *Tex. Heart Inst. J.*, **21**, 22–29.
20. Pepin, M., Schwarze, U., Superti-Furga, A. and Byers, P.H. (2000) Clinical and genetic features of Ehlers-Danlos syndrome type IV, the vascular type. *N. Engl. J. Med.*, **342**, 673–680.
21. Schwarze, U., Schievink, W.I., Petty, E., Jaff, M.R., Babovic-Vuksanovic, D., Cherry, K.J., Pepin, M. and Byers, P.H. (2001) Haploinsufficiency for one COL3A1 allele of type III procollagen results in a phenotype similar to the vascular form of Ehlers-Danlos syndrome, Ehlers-Danlos syndrome type IV. *Am. J. Hum. Genet.*, **69**, 989–1001.
22. Plancke, A., Holder-Espinasse, M., Rigau, V., Manouvrier, S., Claustres, M. and Khau Van Kien, P. (2009) Homozygosity for a null allele of COL3A1 results in recessive Ehlers-Danlos syndrome. *Eur. J. Hum. Genet.*, **17**, 1411–1416.
23. Zhang, M.C., He, L., Giro, M., Yong, S.L., Tiller, G.E. and Davidson, J.M. (1999) Cutis laxa arising from frameshift mutations in exon 30 of the elastin gene (ELN). *J. Biol. Chem.*, **274**, 981–986.
24. Tassabehji, M., Metcalfe, K., Hurst, J., Ashcroft, G.S., Kielty, C., Wilmot, C., Donnai, D., Read, A.P. and Jones, C.J. (1998) An elastin gene mutation producing abnormal tropoelastin and abnormal elastic fibres in a patient with autosomal dominant cutis laxa. *Hum. Mol. Genet.*, **7**, 1021–1028.
25. Szabo, Z., Crepeau, M.W., Mitchell, A.L., Stephan, M.J., Puntel, R.A., Yin Loke, K., Kirk, R.C. and Urban, Z. (2006) Aortic aneurysmal disease and cutis laxa caused by defects in the elastin gene. *J. Med. Genet.*, **43**, 255–258.
26. Hucthagowder, V., Sausgruber, N., Kim, K.H., Angle, B., Marmorstein, L.Y. and Urban, Z. (2006) Fibulin-4: a novel gene

for an autosomal recessive cutis laxa syndrome. *Am. J. Hum. Genet.*, **78**, 1075–1080.
27. Dasouki, M., Markova, D., Garola, R., Sasaki, T., Charbonneau, N.L., Sakai, L.Y. and Chu, M.L. (2007) Compound heterozygous mutations in fibulin-4 causing neonatal lethal pulmonary artery occlusion, aortic aneurysm, arachnodactyly, and mild cutis laxa. *Am. J. Med. Genet. A*, **143A**, 2635–2641.
28. Lee, V.S., Halabi, C.M., Hoffman, E.P., Carmichael, N., Leshchiner, I., Lian, C.G., Bierhals, A.J., Vuzman, D., Brigham Genomic, M., Mecham, R.P. *et al.* (2016) Loss of function mutation in LOX causes thoracic aortic aneurysm and dissection in humans. *Proc. Natl. Acad. Sci. U. S. A.*, **113**, 8759–8764.
29. Guo, D.C., Regalado, E.S., Gong, L., Duan, X., Santos-Cortez, R.L., Arnaud, P., Ren, Z., Cai, B., Hostetler, E.M., Moran, R. *et al.* (2016) LOX mutations predispose to thoracic aortic aneurysms and dissections. *Circ. Res.*, **118**, 928–934.
30. Thompson, R.W., Liao, S. and Curci, J.A. (1997) Vascular smooth muscle cell apoptosis in abdominal aortic aneurysms. *Coron. Artery Dis.*, **8**, 623–631.
31. Yeung, K.K., Bogunovic, N., Keekstra, N., Beunders, A.A., Pals, J., van der Kuij, K., Overwater, E., Wisselink, W., Blankensteijn, J.D., van Hinsbergh, V.W. *et al.* (2017) Transdifferentiation of human dermal fibroblasts to smooth muscle-like cells to study the effect of MYH11 and ACTA2 mutations in aortic aneurysms. *Hum. Mutat.*, **38**, 439–450.
32. Bruijn, L.E., van den Akker, B.E.W.M., van Rhijn, C.M., Hamming, J.F. and Lindeman, J.H.N. (2020) Extreme diversity of the human vascular mesenchymal cell landscape. *J. Am. Heart Assoc.*, **9**, e017094.
33. Malloy, L.E., Wen, K.K., Pierick, A.R., Wedemeyer, E.W., Bergeron, S.E., Vanderpool, N.D., McKane, M., Rubenstein, P.A. and Bartlett, H.L. (2012) Thoracic aortic aneurysm (TAAD)-causing mutation in actin affects formin regulation of polymerization. *J. Biol. Chem.*, **287**, 28398–28408.
34. Rockey, D.C., Weymouth, N. and Shi, Z. (2013) Smooth muscle alpha actin (Acta2) and myofibroblast function during hepatic wound healing. *PLoS One*, **8**, e77166.
35. Lee, H.W., Park, Y.M., Lee, S.J., Cho, H.J., Kim, D.H., Lee, J.I., Kang, M.S., Seol, H.J., Shim, Y.M., Nam, D.H. *et al.* (2013) Alpha-smooth muscle actin (ACTA2) is required for metastatic potential of human lung adenocarcinoma. *Clin. Cancer Res.*, **19**, 5879–5889.
36. Lu, H., Fagnant, P.M., Bookwalter, C.S., Joel, P. and Trybus, K.M. (2015) Vascular disease-causing mutation R258C in ACTA2 disrupts actin dynamics and interaction with myosin. *Proc. Natl. Acad. Sci.*, **112**, E4168—E4177.
37. Kwartler, C.S., Chen, J., Thakur, D., Li, S., Baskin, K., Wang, S., Wang, Z.V., Walker, L., Hill, J.A., Epstein, H.F. *et al.* (2014) Overexpression of smooth muscle myosin heavy chain leads to activation of the unfolded protein response and autophagic turnover of thick filament-associated proteins in vascular smooth muscle cells. *J. Biol. Chem.*, **289**, 14075–14088.
38. Kuang, S.Q., Kwartler, C.S., Byanova, K.L., Pham, J., Gong, L., Prakash, S.K., Huang, J., Kamm, K.E., Stull, J.T., Sweeney, H.L. *et al.* (2012) Rare, nonsynonymous variant in the smooth muscle-specific isoform of myosin heavy chain, MYH11, R247C, alters force generation in the aorta and phenotype of smooth muscle cells. *Circ. Res.*, **110**, 1411–1422.
39. Pannu, H., Tran-Fadulu, V., Papke, C.L., Scherer, S., Liu, Y., Presley, C., Guo, D., Estrera, A.L., Safi, H.J., Brasier, A.R. *et al.* (2007) MYH11 mutations result in a distinct vascular pathology driven by insulin-like growth factor 1 and angiotensin II. *Hum. Mol. Genet.*, **16**, 2453–2462.
40. Hu, B., Wu, Z. and Phan, S.H. (2003) Smad3 mediates transforming growth factor-beta-induced alpha-smooth muscle actin expression. *Am. J. Respir. Cell Mol. Biol.*, **29** 397–404.
41. Vardouli, L., Vasilaki, E., Papadimitriou, E., Kardassis, D. and Stournaras, C. (2008) A novel mechanism of TGFbeta-induced actin reorganization mediated by Smad proteins and Rho GTPases. *FEBS J.*, **275**, 4074–4087.
42. Qiu, P., Feng, X.H. and Li, L. (2003) Interaction of Smad3 and SRF-associated complex mediates TGF-beta1 signals to regulate SM22 transcription during myofibroblast differentiation. *J. Mol. Cell. Cardiol.*, **35**, 1407–1420.
43. van der Pluijm, I., van Vliet, N., von der Thusen, J.H., Robertus, J.L., Ridwan, Y., van Heijningen, P.M., van Thiel, B.S., Vermeij, M., Hoeks, S.E., Buijs-Offerman, R. *et al.* (2016) Defective connective tissue remodeling in Smad3 mice leads to accelerated aneurysmal growth through disturbed downstream TGF-beta signaling. *EBioMedicine*, **12**, 280–294.
44. Choquet, D., Felsenfeld, D.P. and Sheetz, M.P. (1997) Extracellular matrix rigidity causes strengthening of integrin-cytoskeleton linkages. *Cell*, **88**, 39–48.
45. Lo, C.M., Wang, H.B., Dembo, M. and Wang, Y.L. (2000) Cell movement is guided by the rigidity of the substrate. *Biophys. J.*, **79**, 144–152.
46. Saez, A., Buguin, A., Silberzan, P. and Ladoux, B. (2005) Is the mechanical activity of epithelial cells controlled by deformations or forces? *Biophys. J.*, **89**, L52–L54.
47. Burger, J., van Vliet, N., van Heijningen, P., Kumra, H., Kremers, G.J., Alves, M., van Cappellen, G., Yanagisawa, H., Reinhardt, D.P., Kanaar, R. *et al.* (2019) Fibulin-4 deficiency differentially affects cytoskeleton structure and dynamics as well as TGFbeta signaling. *Cell. Signal.*, **58**, 65–78.
48. Franken, R., den Hartog, A.W., Radonic, T., Micha, D., Maugeri, A., van Dijk, F.S., Meijers-Heijboer, H.E., Timmermans, J., Scholte, A.J., van den Berg, M.P. *et al.* (2015) Beneficial outcome of losartan therapy depends on type of FBN1 mutation in Marfan syndrome. *Circ. Cardiovasc. Genet.*, **8**, 383–388.
49. den Hartog, A.W., Franken, R., van den Berg, M.P., Zwinderman, A.H., Timmermans, J., Scholte, A.J., de Waard, V., Spijkerboer, A.M., Pals, G., Mulder, B.J. *et al.* (2016) The effect of losartan therapy on ventricular function in Marfan patients with haploinsufficient or dominant negative FBN1 mutations. *Neth. Heart J.*, **24**, 675–681.
50. Schindelin, J., Arganda-Carreras, I., Frise, E., Kaynig, V., Longair, M., Pietzsch, T., Preibisch, S., Rueden, C., Saalfeld, S., Schmid, B. *et al.* (2012) Fiji: an open-source platform for biological-image analysis. *Nat. Methods*, **9**, 676–682.
51. Boudaoud, A., Burian, A., Borowska-Wykret, D., Uyttewaal, M., Wrzalik, R., Kwiatkowska, D. and Hamant, O. (2014) FibrilTool, an ImageJ plug-in to quantify fibrillar structures in raw microscopy images. *Nat. Protoc.*, **9**, 457–463.
52. Lowry, O.H., Rosebrough, N.J., Farr, A.L. and Randall, R.J. (1951) Protein measurement with the Folin phenol reagent. *J. Biol. Chem.*, **193**, 265–275.
53. Das, A.M., Eggermont, A.M. and ten Hagen, T.L. (2015) A ring barrier-based migration assay to assess cell migration in vitro. *Nat. Protoc.*, **10**, 904–915.
54. Bogunovic, N., Meekel, J.P., Micha, D., Blankensteijn, J.D., Hordijk, P.L. and Yeung, K.K. (2019) Impaired smooth muscle cell contractility as a novel concept of abdominal aortic aneurysm pathophysiology. *Sci. Rep.*, **9**, 6837.